A Systematic Study of the Structure and Bonding of Halogens on Low-Index Transition Metal Surfaces

Annapaola Migani and Francesc Illas*

Departament de Química Física & CeRQT, Universitat de Barcelona & Parc Científic de Barcelona, C/Martí i Franquès 1, E-08028 Barcelona, Spain

Received: January 19, 2006; In Final Form: March 24, 2006

The structure and bonding of halogens on various transition metal low-index surfaces has been studied by means of density functional theory (DFT) calculations using periodic slabs to model the surface. This approach is shown to be capable of reproducing available experimental data of naked and halogen-covered surfaces. Periodic trends are discerned and discussed for several properties, including metal−halogen bond distances and vibrational frequencies, adsorption energies, and bond ionicities, which have been evaluated by a Bader population analysis of the corresponding density. A simple correlation is discerned, relating the bond ionicity to the metal work function, so that higher work function surfaces are associated with more covalent bonding. Periodic trends in bond ionicities and metal−halogen vibrational frequencies are in harmony with corresponding data derived in an electrochemical environment, indicating that the metal−halogen bonding in vacuum share some features with the electrode metal surface−halogen bonding.

1. Introduction

The interaction of halogens on metal surfaces represents one of the prototype examples of both surface science[1−7] and electrochemistry.[8−10] Halogens on metal surfaces in ultrahigh vacuum (UHV) conditions usually result in well-ordered phases,[11] making accurate structural determination possible with a wide variety of techniques. This is the case for Cl on Cu(111), where a clear $(\sqrt{3}\times\sqrt{3})$ *R*30° pattern is observed.[11] However, the situation has been already less clear for Cl on Ag(111) although the structure has been solved long ago.[11] Nevertheless, even for these in principle simple systems, the number of experiments is quite limited and structural data for halogens on metal surfaces seems to be restricted to Cl on various Cu[5,6,12−14] and Ag[15−22] low-index surfaces and also to the $(\sqrt{3}\times\sqrt{3})$ *R*30° pattern obtained for 0.33 monolayer (ML) coverage of Cl and I on the Cu(111),[23−27] Rh(111),[3,28] Pd(111),[29,30] and Ag(111)[2,27,31−35] metal surfaces.

In the case of electrochemistry, the amount of experimental structural data is even more limited due to the complexity of the electrochemical environment. Nevertheless, important progress has been made thanks to the development of in situ spectroscopic techniques[36−39] and to the use of single-crystal electrodes.[40,41] A rather systematic study concerning the adsorption of Cl and Br on Pd, Rh, Pt, Cu, Ag, and Au polycrystalline surfaces in an electrochemical environment was reported by Mrozek and Weaver.[42,43] These authors used surface-enhanced Raman spectroscopy (SERS) to derive vibrational frequencies and force constants for the systems described above and compared their results with theoretical estimates obtained from density functional theory (DFT) calculations carried out for cluster models. From this study, some important conclusions regarding the influence of the metal surface on the nature of the chemisorption bond already emerge although the authors being well aware of the limited set of cases studied stated that a systematic study was highly desirable.

Halogens on metals have also been a trial field for many theoretical techniques, which go from simple empirical quantum chemical models[44] to ab initio cluster model studies based either on Hartree−Fock[45−51] (HF) or various implementations of DFT.[52,53] Pacchioni et al. used methods of analysis of the chemisorption bond of halogens on rather small cluster model representations of Ag(111).[46] These techniques included the constrained-space orbital variation method[54−56] and the analysis of dipole moment curves.[57] They concluded that the bond is almost entirely ionic. A similar conclusion was reached using the same techniques but for halides on mercury.[48,49] Notwithstanding, Pacchioni already found substantial difference in the interaction of halides on Ag(100) and Pt(100),[47] although to reach more general conclusions, it is necessary to consider a larger number of cases. Koper and van Santen[53] used different population analysis and also the inspection of dipole moment curves and concluded that, in vacuum, the interaction decreases from I to F for all metals and that the degree of charge transfer may be very different from one halogen to the other. A very large ionicity was found for F and Cl and a nearly zero charge transfer for I. The differences found between these earlier studies may be due to the use of different methods, HF or DFT, to obtain the ground state energy and charge density and also to the use of cluster models of different size, which may affect the description of the surface electronic structure. Earlier studies strongly suggest that the qualitative description of the chemisorption bond arising from HF studies or from methods that include electronic correlations effects is essentially the same.[58,59] There is also compelling evidence that qualitative trends can be obtained from cluster models.[60−62] However, for a proper comparison between different halogens on a given metal surface or for a given halogen on different metal surfaces, it is necessary to guarantee a similar description for all systems. A better model for the surface will surely result in a better and more accurate description of the interaction. For well-ordered surface structures such as those described above, a periodic model seems to be more convenient. A few studies using periodic models have also

* Corresponding author. E-mail: francesc.illas@ub.edu.

10.1021/jp060400u CCC: $33.50
Published on Web 06/01/2006

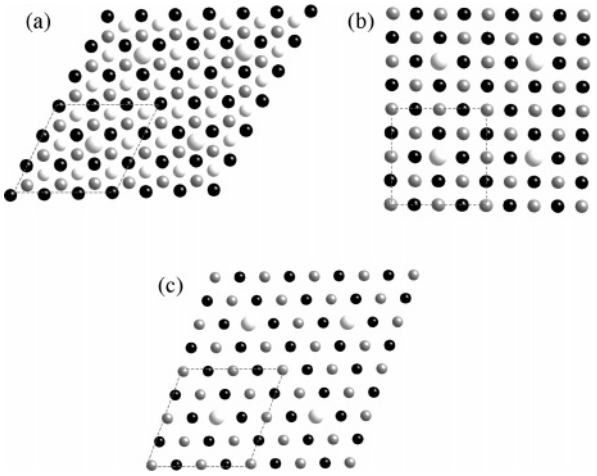

Figure 1. Unit cell considered to model intermediate coverage for halogen adsorption on transition metal surfaces. (a) The (111) surface 3×3 unit cell with the halogen atom placed at the 3-fold fcc site and 0.11 ML coverage; (b) the (100) surface 2×2 unit cell with the halogen placed at the 4-fold hollow site and 0.125 ML coverage; (c) the (110) surface 2×2 unit cell with the halogen placed at the hollow site and 0.125 ML coverage.

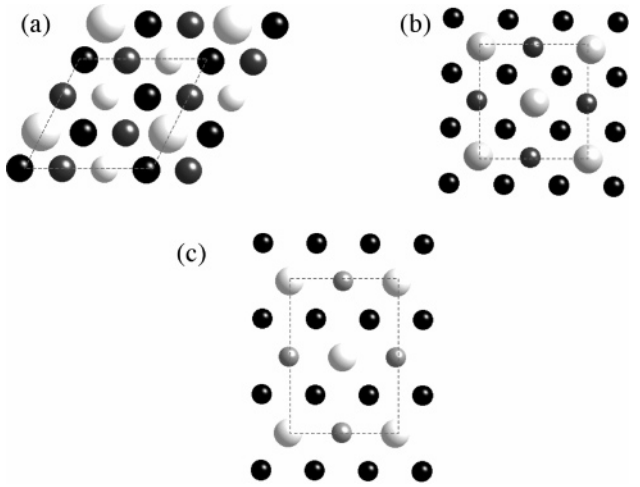

Figure 2. Surface structures used to model Cl adsorption on Cu and Ag at high coverage. a) The $(\sqrt{3}\times\sqrt{3})$ *R*30°−Cl supercell for the (111) surface with the chlorine atom placed at the 3-fold fcc site and 0.33 ML coverage; (b) the c(2×2)-Cl supercell for the (100) surface with the chlorine placed at the 4-fold hollow site and 0.5 ML coverage; (c) the c(2×2)-Cl supercell for the (110) surface the chlorine placed at the hollow site and 0.5 ML coverage.

been reported, but these are limited to the interaction of Cl with different metal surfaces.[63−67]

In view of the insufficient existing data, a systematic study of the interaction of halogens with metal surfaces seems to be necessary. The main aim of this paper is precisely to provide such a systematic study. To this end we consider the interaction of F, Cl, Br, and I with the low-index ((111), (100), and (110)) surfaces of Cu, Rh, Pd, Ag, Pt, and Au and carry out DFT calculations on suitable slab models. Various properties such as atomic structures, adsorption energies, vibrational frequencies, and net charges are obtained and analyzed. The rather large set of calculated data is then used to unravel systematic trends for the interaction of halogens with metal surfaces.

2. Surface Models

The (100), (110), and (111) low-index surfaces of Cu, Rh, Pd, Ag, Pt, and Au were modeled through a periodic three-dimensional supercell approach with slab models containing four atomic layers. The vacuum region between the periodically repeated slabs was at least 12 Å. Halogen (F, Cl, Br, and I) adsorption on these surfaces was studied by placing the adsorbate on one side of the slab surfaces. Both the halogen and the two uppermost atomic layers were allowed to relax completely, and the remaining two layers were fixed at their bulk-like position, which in turn was obtained from periodic calculations for the bulk materials.

To model intermediate coverage, a 2×2 supercell was used for the (100) and (110) surfaces, whereas a 3×3 unit cell was used for the (111) ones. In the (111) surfaces, the halogen atom was placed at the 3-fold fcc site, thus directly above a metal atom in the third layer (Figure 1a). A 4-fold hollow site was considered for the (100) surface (Figure 1b), and also a hollow site was considered for the (110) surface (Figure 1c). This choice is justified because the hollow site considered is in most cases the experimentally observed one and hence the most stable at least at 0.33 ML for the (111) surface, and 0.5 ML for the (100) and (110) surfaces. With the unit cells described above, the resulting coverage state is 0.111 ML for (111) and 0.125 ML for both the (100) and (110) surfaces. Hence, the halogen overlayers considered in the present work do not necessarily correspond to those experimentally observed for the different metal surfaces and the computed properties cannot be directly compared to experimental data. Therefore, a second set of calculations was carried out for the Ag(111) and Cu(111) surfaces, with chlorine absorbed at coverage of 0.33 ML in a $(\sqrt{3}\times\sqrt{3})$ *R*30° supercell (Figure 2a). Calculations were also carried out for the c(2×2)-Cl overlayer on the Cu(100) and Ag(100) surfaces (Figure 2b) and a c(2×2)-Cl overlayer on the Cu(110) and Ag(110) surfaces (Figure 2c), which correspond to 0.5 ML coverage. This additional calculations effectively simulate available experimental data[2,5,6,12−24] and, therefore, provide reliable benchmarks, thus allowing us to check the accuracy of the theoretical methodology used throughout the present study. In addition, for comparative purposes, low coverage was also investigated for the (100) surface of Cu and Pt by studying a 3×3 supercell, which leads to 0.056 ML coverage. Comparison of the data obtained with different supercells permits the study of the modification of the structure and electronic properties induced by coverage.

3. Computational Details

The atomic and electronic structure of the halogen overlayers on the different low-index metal surfaces described above was obtained by means of DFT calculations carried out using the Vienna ab initio simulation program (VASP).[68−70] The DFT calculations were performed using the generalized gradient approximation (GGA) with the exchange-correlation potential developed by Perdew et al.[71] The effect of the exchange-correlation potential was tested in a few selected systems (see Subsection 4.b.). To this end, we used the Perdew−Burke−Ernzerhof[72] implementation of GGA (hereafter referred to as GGA-PBE) and local density approach (LDA) within the Ceperly−Alder version[73] as implemented in VASP. The comparison between calculated bulk properties (Table 1) and experiment[74,75] clearly evidences, as expected, the superiority of the GGA potential over LDA. The LDA tends to underestimate the lattice constant, and as a consequence, the bulk modulus and cohesive energy are exceedingly large. Unless otherwise specified, calculations were carried out using the standard (nonspin polarized) Kohn−Sham formalism.

TABLE 1: Ground State Properties of Bulk Cu and Ag[a]

	a_0		B_0		E_{coh}	
	Cu	Ag	Cu	Ag	Cu	Ag
LDA	3.527	4.019	1.99	1.32	4.52	3.61
GGA	3.639	4.161	1.38	0.91	3.50	2.55
GGA-PBE	3.641	4.167	1.38	0.90	3.47	2.49
experiment[74,75]	3.615	4.085	1.37	1.01	3.50	2.96

[a] a_0 (in Å) is the lattice parameter. B_0 (in mbar) is the bulk modulus. E_{coh} (in eV/atom) is the absolute value of the metal cohesive energy.

The Kohn−Sham one-electron wave functions were expanded on the basis of plane waves with kinetic energy below 420 eV. A ($5 \times 5 \times 1$) Monkhorst−Pack grid of special k points was used for integration in the reciprocal space. The projector-augmented wave (PAW) method developed by Blöch[76] was used to reproduce the atomic core effects in the electronic density of the valence electrons. The PAW is essentially an all-electron frozen core method combining the accuracy of all electron methods, such as the full potential linearized plane wave method, and the computational simplicity of the pseudopotential approach, especially in the implementation of Kresse and Joubert.[77] The residual minimization method direct inversion in the iterative subspace (RMM-DIIS) algorithm was used for the minimization of the Kohn−Sham one-electron orbitals. A quasi-Newton algorithm was used to relax the atomic position in the geometry optimization. This algorithm utilizes the forces and the stress tensor to determine the search direction for finding the equilibrium positions. The order-2 Methfessel−Paxton method with a smearing width of 0.20 eV was used to determine how the partial occupancies are set for each one-electron wave function in the slab geometry optimizations. For the accurate computation of the total energies, the tetrahedron method with Blöch corrections was used. Hence, the final energies are not affected by any smearing.

The degree of convergence of the calculations was tested against the density of k-point sampling within the Brillouin zone, the plane-wave cutoff, and the width of the vacuum layer between the slabs. To this end, a number of calculations for the Pt(111) surface and halogen-covered Pt(111) surface was undertaken with different values of these parameters. The test calculations carried out with a vacuum layer of at least 15 Å, with an energy cutoff (E_{cut}) of 500 eV and a ($7 \times 7 \times 1$) Monkhorst−Pack k-point mesh confirmed the results obtained with the set of parameters described above, yielding similar energies and geometries.

The standard dipole correction was used always to compute energetic and structural properties of clean and halogen-covered surfaces. The work function of the metal surfaces and halogen-covered surfaces was calculated as usual by subtracting the Fermi energy from the electrostatic potential at the vacuum. The latter was obtained by computing the electrostatic potential in the direction perpendicular to the surface and taking the value where it became nearly constant. The adsorption energies were computed by subtracting from the total energy of the system with the adatom those of the clean surface and isolated halogen atom. The latter was computed by an appropriate spin-polarized calculation of the atom placed in a sufficiently large asymmetric box.

Estimation of the degree of ionicity of the adatom metal−surface bond is provided by carrying out an atoms-in-molecules (AIM) analysis of the charge density.[78] In the AIM approach, the total density is partitioned in different nonoverlapping regions defining the atomic basins. The atomic basins are separated from each other by surfaces with zero gradient of the electron density. Numerical integration of the density for each basin provides an estimate of the total population on a given atom that is almost independent of atomic basis set and can indeed be used within a plane-wave basis set where other population analyses, which are often based on the use of atom-centered basis functions, cannot be carried out.

TABLE 2: Summary of the Calculated Properties of the Clean (100) Surface of Cu, Rh, Pd, Ag, Pt, and Au Using a 2 × 2 Supercell[a]

	(100)			
	δ_{12}	δ_{23}	E_{sur}	Φ
Cu	−0.048	0.024	1.42	4.53 (4.59)[122]
	−2.64% (−2.0%)[79]	1.31% (+1.0%)[79]		
Rh	−0.071	−0.005	2.38	5.22
	−3.70% (+0.5%)[88]	−0.28% (0.0%)[88]		
Pd	−0.022	0.005	1.53	5.12
	−1.10% (+3.1%)[86]	0.27% (−1.0%)[86]		
Ag	−0.036	0.016	0.84	4.16 (4.64)[122]
	−1.74% (0.0%)[87]	0.75% (0.0%)[87]		
Pt	−0.054	−0.031	1.89	5.75
	−2.72%	−1.55%		
Au	−0.027	0.008	0.93	5.02 (5.47)[122]
	−1.31%	0.36%%		

[a] Experimental values for the surface energy for isotropic crystals are: 1.79 J/m^2 (Cu), 2.66 J/m^2 (Rh), 2.00 J/m^2 (Pd), 1.25 J/m^2 (Ag), 2.49 J/m^2 (Pt), and 1.51 J/m^2 (Au).[121] Experimental values for the work function for polycrystalline samples are: 4.65 eV(Cu), 4.98 eV (Rh), 5.12 eV (Pd), 4.26 eV (Ag), 5.65 eV (Pt), and 5.1 eV (Au).[122] δ_{12} and δ_{23} (in Å and in %) are the average interlayer relaxations of the first two layers relative to the computed bulk interlayer spacing. E_{sur} (in J/m^2) is the surface energy. Φ (in eV) is the surface work function. Available experimental data are given in parentheses.

4. Assessment of the Computational Model

In this section, we carefully examine the performance of the surface models and computational approach described above. To this end, we first present a systematic analysis of the results corresponding to the clean surfaces and compare with available experimental data. In a second step, we take the case of Cl adsorption on the low-index surfaces of Cu and Ag to calibrate the accuracy of the present calculations and the reliability of the models chosen to represent the interaction of halogens with these surfaces. Hence, we investigate the effect of the exchange-correlation potential used in the DFT calculations and also the possible influence of coverage. The choice of Cl on these metal surfaces is justified by the extensive literature available for these systems either from the experimental or computational points of view.

4.a. Calculated Properties of the Clean Surfaces. A brief summary of the main results for the clean surfaces is reported in Tables 2−4. A common trend generally observed for the surface relaxation predicted from the DFT calculations for the (100) and (110) surfaces of metals with a face-centered cubic (fcc) crystal structure consists of a contraction of the first (δ_{12}) and an expansion of the second (δ_{23}) interlayer distances. This trend was found for the Cu(100) surface by several experimental techniques such as medium-energy ion scattering (MEIS),[79,80] low-energy electron diffraction (LEED),[81−84] or spin-polarized (SP) LEED.[85] Calculations also predict a contraction/expansion trend for the (100) surface of Ag and Pd. However, these theoretical predictions do not agree with experiments (Table 2). In fact, a LEED study[86] of a clean Pd(100) surface reported an expansion of the first and a contraction of the second interlayer spacing. Similarly, a LEED study[87] of a clean Ag-(100) surface found no multilayer relaxation for either the first

TABLE 3: Summary of the Calculated Properties of the Clean (110) Surface of Cu, Rh, Pd, Ag, Pt, and Au Using a 2 × 2 Supercell[a]

	(110)			
	δ_{12}	δ_{23}	E_{sur}	Φ
Cu	−0.131	0.064	1.45	4.49(4.48)[122]
	−10.17% (−8.5%)[89]	4.94% (2.3%)[89]		
Rh	−0.120	−0.012	2.35	4.69
	−8.85%	−0.86%		
Pd	−0.101	0.048	1.55	5.02
	−7.22%	3.42%		
Ag	−0.148	0.071	0.87	4.25 (4.52)[122]
	−10.09% (−7.8%)[93]	4.83% (4.3%)[93]		
Pt	−0.153	0.087	1.88	5.46
	−10.85%	6.20%		
Au	−0.217	0.126	0.92	4.99(5.37)[122])
	−14.68%	8.52%		

[a] For the surface energy for isotropic crystals and work function for polycrystalline samples experimental values see footnote of Table 1. δ_{12} and δ_{23} (in Å and in %) are the average interlayer relaxations of the first two layers relative to the computed bulk interlayer spacing. E_{sur} (in J/m^2) is the surface energy. Φ (in eV) is the surface work function. Available experimental data are given in parentheses.

TABLE 4: Summary of the Calculated Properties of the Clean (111) Surface of Cu, Rh, Pd, Ag, Pt, and Au Using a 3 × 3 Supercell[a]

	(111)			
	δ_{12}	δ_{23}	E_{sur}	Φ
Cu	−0.027	0.009	1.11	4.98 (4.78)[122]
	−1.89% (−1.0%)[100]	−0.37% (−0.2%)[100]		
Rh	−0.027	−0.051	1.72	5.16
	−1.37% (−1.39%)[109]	−2.27% (−1.39%)[109]		
Pd	0.009	−0.010	1.17	5.38
	0.26% (1.78%)[109]	−0.44% (−0.89%)[109]		
Ag	−0.002	0.001	0.68	4.54 (4.74)[122]
	−0.55% (−2.5%)[106]	0.21% (+0.6%)[106]		
Pt	0.021	−0.015	1.34	5.80 (5.7)[122]
	0.93% (0.5%)[111]	−0.65%		
Au	0.010	−0.011	0.69	5.22 (5.31)[122]
	−0.13%	−0.99%		

[a] For the surface energy for isotropic crystals and work function for polycrystalline samples experimental values see footnote of Table 1. δ_{12} and δ_{23} (in Å and in %) are the average interlayer relaxations of the first two layers relative to the computed bulk interlayer spacing. E_{sur} (in J/m^2) is the surface energy. Φ (in eV) is the surface work function. Available experimental data are given in parentheses.

or the second interlayer spacing. The theoretical data for the Rh(100) surface also deviate from experiments. A LEED study[88] of Rh(100) found a slight first-layer expansion, and no relaxation for the second interlayer spacing, while an inward relaxation is predicted theoretically for both the first and the second layers. The origin of these differences between experimental and calculated values is unclear, and we suggest that this is mostly due to temperature effects and sample preparation. This claim is supported by the calculated relaxation values for Cu(110) and Ag(110), which agree well with the experimental trend observed by LEED[83,89−92] and high-energy ion scattering (HEIS)[89] measurements for the Cu(110) surface and also by HEIS[93] measurements, shadow- cone-enhanced secondary ion mass spectroscopy (SIMS),[94] Rutherford backscattering,[95] and LEED[83] experiments for the Ag(110) surface, although earlier LEED studies[96−99] for Ag(110) reported a contraction of the first-layer spacing only. The rest of the (110) surfaces relax in a manner similar to Cu(110) and Ag(110).

Table 4 shows that the theoretical data also reproduce most of the trends found experimentally for Rh(111), Ag(111), and Cu(111). The structure of Ag(111) and Cu(111) was studied as a function of the temperature. A MEIS study for Cu(111)[100] found first and second interlayer spacing contractions at room temperature. This is in agreement with the predicted calculated trend. Notice, however, that earlier LEED studies[101−105] for Cu(111) reported a contraction of the first-layer spacing only. A MEIS study of the Ag(111) structure reported a contraction of the first and an expansion of the second interlayer spacing[106] at 300 K, again in agreement with the present results, and at variance with previous LEED data,[107] which reported a contraction of both the first and second interlayer spacing, at a temperature of 330 K. A contraction of the first interlayer spacing was also measured using X-ray scattering.[108] Similarly, it seems very likely that the Rh(111) outermost atomic layers contract. A LEED structural investigation[109] of Rh(111) predicted a contraction of both the first and second interlayer spacing, although an earlier LEED study found an inward relaxation of the topmost layer.[110] From the preceding discussion, one can conclude that, for the Cu, Ag, Rh (111) surfaces, the first interlayer spacing is contracted even at room temperature. The Pt(111) surface represents an exception because SPLEED measurements[111] established that the Pt(111) surface undergoes a very slight outward relaxation of the topmost atomic layer, thus confirming previous MEIS[112−114] and LEED[115−118] studies. The structure of the Pd(111) surface is also found to be different from those of Cu, Ag, and Rh(111). In fact, LEED structural determinations[109,119,120] of Pd(111) suggested an expansion of the first and a contraction of the second interlayer spacing. The present calculated surface relaxation for these surfaces confirm the differences with respect to Cu, Ag, and Rh(111). Notice that the agreement between calculated and experimental results is less satisfactory for Ag(100), Pd(100), and Rh(100), although as already discussed in previous work, the calculated data are in agreement with calculations by others.[66] Therefore, the present calculated surface relaxation for the different crystal faces of these six transition metals appear to be accurate enough, especially for the present purposes.

Apart from the surface relaxation, Tables 2−4 also include results for the surface energy and work function and compare them with available experimental data.[121,122] Surface energies are calculated as in eq 1

$$E_{sur} = \frac{1}{2S}[E_{slab}(n) - nE_{bulk}] \quad (1)$$

where E_{slab} is the energy of the slab, E_{bulk} that of the bulk, n the number of atoms in the slab unit cell, and S the unit cell surface area. The experimental surface energies,[121]1.33 J/m^2 (Cu), 2.15 J/m^2 (Rh), 1.42 J/m^2 (Pd), 0.80 J/m^2 (Ag), 1.70 J/m^2 (Pt), and 0.84 J/m^2 (Au), correspond to isotropic crystal and, thus, do not provide information for the surface energy of a particular surface face. Nevertheless, the calculated surface energy trend for the different low-index surfaces compares well with the experimental one for the isotropic crystals. The experimental work function is available for the (111), (100), and (110) surfaces of the group 11 metals and for polycrystalline samples of all metals considered here. The comparison between the calculated value for a specific surface with the corresponding experimental value shows noticeable differences, which go from 0.22% for Cu(110) to 10.34% for Ag(100) with an average deviation of less than 5%. Interestingly enough, the correlation between experiment and theory is extremely good when comparing the work function values for polycrystalline samples to the calculated average values over the three low-index surfaces. In this case, the experimental trend is quantitatively reproduced and the deviation is always in absolute value less than 1%.

TABLE 5: Adsorption of Cl on Cu and Ag Low-Index Surfaces as Predicted from DFT Calculations Carried out for the Supercells Defined in Figure 2 Corresponding to 0.33, 0.5, and 0.5 ML Coverage for the (111), (110), and (100) Surfaces, Respectively[a]

	Cu(111)			Cu(100)			Cu(110)		
	r_{NN}	E_{ads}	N_e	r_{NN}	E_{ads}	N_e	r_{NN}	E_{ads}	N_e
GGA	2.388	−3.34	7.47	2.462	−7.15	7.49	2.670	−3.30	7.56
GGA-PBE	2.386	−3.24	7.47	2.469	−7.00	7.50	2.669	−3.19	7.56
LDA	2.315	−4.02	7.44	2.383	−8.55	7.46	2.575	−4.00	7.53
experiment	2.38[b]−2.48[c][127]			2.39[d]−2.42[e][5]					

	Ag(111)			Ag(100)			Ag(110)		
	r_{NN}	E_{ads}	N_e	r_{NN}	E_{ads}	N_e	r_{NN}	E_{ads}	N_e
GGA	2.628	−3.02	7.46	2.718	−6.61	7.39	2.935	−3.11	7.53
GGA-PBE	2.629	−2.91	7.46	2.720	−6.47	7.39	2.940	−3.00	7.55
LDA	2.555	−3.61	7.42	2.632	−7.84	7.35	2.842	−3.70	7.53
experiment	2.70[b][2]			2.69[19]			2.50[c]−2.90[d][22]		

[a] r_{NN} (in Å) is the nearest-neighbor chlorine distance to the surface metal atom. E_{ads} (in eV) is the adsorption energy. N_e corresponds to the total population on the adsorbate (in units of |e|) derived from a Bader analysis of the DFT charge density. [b] Referred to range of coverage from 0.17 to 0.33 ML. [c] Referred to 0.08 ML coverage. [d] Referred to 0.50 ML coverage. [e] Referred to 0.12 ML coverage.

4.b. Cl on Cu and Ag Low-Index Surfaces. In this section, an extensive study of the Cl adsorption on the Cu and Ag low-index surfaces is presented, which is aimed at unraveling the dependence of the calculated results for the adsorbate−surface structure and for the nature of the chemisorption bond on the exchange-correlation potential. For this purpose, one needs to compare with available experimental data and, consequently, the slab geometries corresponding to the adsorption structures found experimentally have been considered. The results of these calculations are summarized in Table 5.

The surface energies calculated at the GGA level for the Cu and Ag surfaces are identical to the corresponding values in Tables 2−4 as expected. This provides an internal consistency test of the model because it shows that this property is not affected by the supercell size. Moreover, the two different implementations of GGA give practically identical results, while the LDA surface energies are found to be always higher than those computed within the GGA.

The structural model used to study the adsorption of Cl on the Cu and Ag(100) surfaces is shown in Figure 2b and corresponds to a c(2×2) arrangement of the Cl atoms at the 4-fold symmetrical hollow of the (100) surface. This model has been confirmed experimentally for both the Cu(100)[5,6,12−14] and Ag(100)[15−19] surfaces. The Cu(100) c(2×2)-Cl structure has been extensively investigated by various experimental techniques. A combination of LEED and photoemission led to a Cu−Cl nearest-neighbor distance r_{NN} of 2.38 Å.[12,13] Similar values were found by two independent surface-extended X-ray adsorption fine structure (SEXAFS) experiments.[5,14] A slightly larger value of 2.42 Å corresponding to a perpendicular distance of the chlorine to the surface plane $r_\perp$ of 1.60 Å was found by an angle-resolved photoemission extended fine structure (ARPEFS) study.[6] When comparing the theoretical structures to the experiments for this surface, the best agreement is found within the LDA approach, which predicts a Cu−Cl r_{NN} of 2.38 Å. This approach gives shorter distances by 0.08 and 0.09 Å than the GGA-PBE methods, respectively. For the Ag(100) c(2×2)-Cl, one finds a Ag−Cl r_{NN} of 2.72 Å at the GGA and GGA-PBE levels with a consistent shorter distance of 2.63 Å at the LDA level. The perpendicular distance from Cl to the surface plane is 1.75 Å (GGA and GGA-PBE) and 1.70 Å (LDA). The LDA values of r_{NN} and $r_\perp$ agree reasonably well with LEED experiments, which reported a Cl−Ag(100) perpendicular distance of 1.72 Å[17] and a Ag−Cl bond length of 2.61 Å.[15] An independent experiment using angle-resolved SIMS reported r_{NN} to be 2.60 Å,[16] in agreement with the LEED measurements. A slightly larger deviation from the experimental data reported above is found at the GGA levels, which predict larger distances. However, a slightly larger r_{NN} distance corresponding to 2.69 Å was found by more recent SEXAFS experiments,[19] which better compares with the GGA results.

Adsorption of Cl on Cu(111) leads to the ordered structure shown in Figure 2a and corresponding to a $(\sqrt{3}\times\sqrt{3})$ *R*30° pattern with the Cl atoms at the 3-fold fcc hollow site and 0.33 ML coverage.[11] This site was also identified as the most stable by previous ab initio periodic DFT calculations for both the Ag(111)−Cl[63,64] and Cu(111)−Cl[65] systems. The experimental determination of the structure arising from the adsorption of Cl on Ag(111) has been more controversial, and several different adsorption patterns have been reported depending on the coverage.[2,11,123−126] However, it seems that, at 0.33 ML, the model structure should correspond to that shown in Figure 2a.[2]

A chlorine−copper interlayer spacing of 1.87 Å corresponding to a chlorine−copper r_{NN} of 2.38 Å was measured by shadow-cone-enhanced SIMS.[127] Normal incidence X-ray standing wave (NIXSW) measurements consistently measured a Cu−Cl top-layer spacing of 1.81 Å.[4,7,23] SEXAFS and photoelectron diffraction studies by the same authors led to a Cu−Cl r_{NN} of 2.39 Å corresponding to a Cu−Cl $r_\perp$ of 1.88 Å.[128,129] These measurements are all consistent with early LEED studies by Goddard and Lambert.[11] It is interesting to note that the Cl−Cu_{NN} distance on Cu(111) is found to be the same on the Cu(100) surface. The calculated GGA distances (2.39 and 1.87 Å for r_{NN} and $r_\perp$, respectively) are in excellent agreement with experiment and with previous calculations[65] that employed the same GGA but made use of a local Gaussian-type basis set. A larger discrepancy is found at the LDA level and, as in the case of the Cu(100) c(2×2)-Cl structure, the LDA calculations predict too-short bond lengths (2.31 and 1.81 Å for r_{NN} and $r_\perp$, respectively). The fact that better agreement with experiment is found for the Cu(100) c(2×2)-Cl structure using the LDA approach, whereas for the Cu(111) $(\sqrt{3}\times\sqrt{3})$ *R*30°-Cl structure, using GGA has to be taken as uncertainties of the results provided by the current implementations of density functional theory and evidence the limitations of the present exchange-correlation potentials. Nevertheless, the numerical differences are small enough so that the calculated results can be taken as rather accurate predictions with some error bars, which for the equilibrium distances do not exceed 0.05 Å. Hence, it is expected that the present calculations may help to solve some controversial results reported in the literature. This is the case of Cl on Ag(111) for which two SEXAFS measurements reported different final structures. One experiment gave the structure of Figure 2a for 0.33 ML coverage and a distance of 2.70 Å between the chlorine adsorbed at the fcc hollow site and the nearest-neighbor Ag atom. Another experiment[1] reported that a sharp $(\sqrt{3}\times\sqrt{3})$ *R*30° pattern at 0.33 ML coverage can only be observed at temperatures below the room temperature and reported a Cl−Ag r_{NN} distance of 2.48 Å at 195 K, although the adsorption site was not determined. The Ag−Cl r_{NN} distance is determined to be 2.63 Å at the GGA levels. The adsorption geometry has been recomputed using the local density approximation, which gives a bond length shorter by 0.08 Å. The GGA perpendicular distance of the chlorine to the surface is 2.0 Å (1.96 Å at the LDA level). The LDA and GGA geometries

are in excellent agreement with previous calculations[63] that employed the Dirac−Slater exchange[130,131] and Perdew and Wang correlation potential and used a local Gaussian-type basis set. However, given the differences between the GGA and LDA calculated values, the present model studies are not able to firmly confirm any of these experiments, although calculations would support the structures reported by Lamble et al.[2] Here, it is worth to point out that recent theoretical work[64] showed that adsorption of chlorine on the Ag(111) surface, even without taking into account surface defects, can lead to a range of energetically similar but structurally very dissimilar chlorine overlayers exhibiting different silver−chlorine bond lengths. Therefore, it appears that the two SEXAFS measurements, instead of being contradicting, are equally valid and should be interpreted as referring to different overlayer structures formed in the experiments. Moreover, de Leeuw et al.[64] found that, in all configurations where Cl atoms are located either at fcc and/or hpc hollow sites, the chlorine−silver bond lengths range from 2.56 to 2.69 Å. Indeed, this is close to the value measured by Lamble et al.[2]

Figure 1c shows the (110) surface covered with a layer of chlorine corresponding to 0.5 ML coverage in a c(2×2) pattern with Cl placed at the 4-fold bonding site. The Cl−Cu nearest-neighbor bond distance (2.67 Å within the GGA and 2.58 Å at the LDA level) is found to be substantially larger than on the (111) and (100) surfaces. The GGA nearest-neighbor bond length for Cl on Ag(110) is 2.94 Å, whereas the LDA prediction is 2.84 Å. These values are larger than those determined for adsorption onto the other low-index faces of silver. SEXAFS structural determinations for Cl on Ag(110) reported r_{NN} to be 2.56 Å at 0.75 ML.[20,21] Another independent study[22] employing shadow-cone SIMS reported a Cl−Ag bond length of 2.50 Å at high-coverage that is in agreement with the SEXAFS experiments. The difference between the computed and measured values of r_{NN} is far too large to be justified in terms of the experimental uncertainty or theoretical error and reflects the fact that the computed and measured values refer to two different physical situations. The SEXAFS experiments indeed pointed out that, at 0.75 ML coverage, the Cl atom is indeed placed at distorted out-of-plane 3-fold sites rather than at the 4-fold bonding site.[20,21]

We end this section by a quick inspection of the adsorption energies for Cl on the Cu and Ag low-index surfaces. The most striking feature is the difference between the LDA and GGA calculated values, the formers being considerably larger than the latters obtained with the in principle more accurate GGA potentials. Overall, the LDA adsorption energies are overestimated by roughly 25% with respect to the GGA values. Also, the PW91 or PBE adsorption energies appear to be close to each other. This is in line with the known trends for adsorption energies reported in the literature and need no further comments.[132] The adsorption energies for the halogen series on the Cu, Rh, Pd, Ag, Pt, and Au low-index surfaces will be considered at length in the forthcoming discussion.

5. General Trends in the Adsorption of Halogens on Cu, Rh, Pd, Ag, Pt, and Au Low-Index Surfaces

In this section, the results for halogen adsorption on the three low-index surfaces of Cu, Rh, Pd, Ag, Pt, and Au are presented and analyzed. The properties chosen to analyze the interaction are the vertical separation between the halogen and the outermost surface layer (Table 6), the total valence population on the halogen obtained through the AIM theory of Bader (Table 7), the nearest-neighbor halogen distance to the surface metal atom (Table 8), the effective halogen radius (Table 9), the work function change induced by the halogen adsorption (Table 10), the vibrational frequency for the motion of the adsorbate perpendicular to the surface (Table 11), and the adsorption energy (Table 12).

TABLE 6: Equilibrium Perpendicular Distance of the Halogen to the Averaged Surface Plane ($r_\perp$) for Halogen Chemisorption on the Three Low-Index Surfaces of Cu, Rh, Pd, Ag, Pt, and Au and Average Value ($\langle r_\perp \rangle$) among the Different Metal Surfaces[a]

		metal						average
	halogen	Cu	Rh	Pd	Ag	Pt	Au	$\langle r_\perp \rangle$
(111)	F	1.531	1.646	1.581	1.650	1.709	1.706	1.637
	Cl	1.921	1.907	1.854	2.052	1.963	2.075	1.962
	Br	2.087	2.065	2.002	2.189	2.103	2.214	2.110
	I	2.292	2.202	2.143	2.383	2.225	2.342	2.265
(110)	F	1.007	1.077	1.042	1.006	1.196	1.120	1.075
	Cl	1.460	1.339	1.185	1.505	1.486	1.662	1.440
	Br	1.596	1.540	1.246	1.640	1.569	1.769	1.560
	I	1.830	1.582	1.356	1.875	1.403	1.866	1.652
(100)	F	1.307	1.416	1.413	1.321	1.519	1.448	1.404
	Cl	1.735	1.614	1.647	1.844	1.695	1.938	1.750
	Br	1.875	1.752	1.762	1.976	1.827	2.042	1.872
	I	2.072	1.892	1.833	2.198	1.881	2.161	2.006

[a] The data refer to 0.111, 0.125, and 0.125 ML coverage for the (111), (110), and (100) surfaces, respectively, corresponding to the structures defined in Figure 1. All distances are in Å.

TABLE 7: Halogen Total Valence Population Obtained from the Bader Analysis for Halogen Chemisorption on the Three Low-Index Surfaces of Cu, Rh, Pd, Ag, Pt, and Au and Average Value ($\langle N_e \rangle$) among the Different Metal Surfaces[a]

		metal						average
	halogen	Cu	Rh	Pd	Ag	Pt	Au	$\langle N_e \rangle$
(111)	F	7.71	7.64	7.64	7.71	7.59	7.63	7.65
	Cl	7.50	7.42	7.36	7.51	7.31	7.39	7.42
	Br	7.39	7.26	7.20	7.41	7.13	7.25	7.27
	I	7.23	7.02	6.94	7.24	6.84	7.04	7.05
(110)	F	7.74	7.69	7.69	7.73	7.64	7.65	7.69
	Cl	7.58	7.53	7.48	7.59	7.37	7.48	7.51
	Br	7.49	7.39	7.31	7.51	7.24	7.37	7.39
	I	7.30	7.14	7.01	7.34	6.83	7.14	7.13
(100)	F	7.75 (7.77)[b]	7.68	7.70	7.74	7.64 (7.64)[b]	7.68	7.70
	Cl	7.50 (7.54)[b]	7.54	7.49	7.56	7.37 (7.36)[b]	7.51	7.50
	Br	7.39 (7.41)[b]	7.32	7.27	7.52	7.24 (7.12)[b]	7.51	7.38
	I	7.30 (7.26)[b]	7.12	7.02	7.29	6.78 (6.92)[b]	7.09	7.10

[a] The data refer to 0.111, 0.125, and 0.125 ML coverage for the (111), (110), and (100) surfaces, respectively, corresponding to the structures defined in Figure 1. Bader populations are in units of $|e|$. [b] Obtained from a calculation with seven atomic layers.

First, let us analyze the variation of the adsorbate−metal vertical distance $r_\perp$ for a given adsorbate on the different metals. Inspection of Table 6 shows that, when considering adsorption of Cl, Br, and I, the largest vertical distances are generally found for the group 11 metals (Cu, Ag, Au), whereas quite smaller vertical distances are found for Rh, Pd, and Pt metals. Another significant feature is that the $r_\perp$ distance increases monotonically down to the group 11, with the largest value thus occurring for adsorption on Au, except when the adatom is iodine. In this case, there is an inversion of the Ag−I and Au−I vertical distances and it is found that $r_\perp$ (Au−I) < $r_\perp$ (Ag−I). The observations above suggest that bond covalence is more prevalent for the group 10 metals (Pd, Pt) and Rh compared with the group 11 metals and also suggest that the bond covalence of the Au/I system is larger than that forthe Ag/I one.

TABLE 8: Equilibrium Nearest-Neighbor Halogen Distance to the Surface Metal Atom (r_{NN}) Halogen Chemisorption on the Three Low-Index Surfaces of Cu, Rh, Pd, Ag, Pt, and Au and Average Value ($\langle r_{NN} \rangle$) among the Different Metal Surfaces[a]

		metal						average
	halogen	Cu	Rh	Pd	Ag	Pt	Au	$\langle r_{NN} \rangle$
(111)	F	2.106	2.246	2.267	2.348	2.374	2.423	2.294
	Cl	2.404	2.452	2.449	2.665	2.550	2.700	2.537
	Br	2.550	2.573	2.558	2.787	2.653	2.804	2.654
	I	2.705	2.684	2.665	2.923	2.738	2.903	2.770
(110)	F	2.443	2.588	2.635	2.732	2.715	3.054	2.695
	Cl	2.651	2.703	2.688	2.946	2.849	3.044	2.814
	Br	2.733	2.804	2.715	3.020	2.890	3.099	2.877
	I	2.871	2.824	2.759	3.151	2.798	3.155	2.926
(100)	F	2.227	2.390	2.422	2.459	2.506	2.543	2.425
	Cl	2.498	2.506	2.557	2.775	2.607	2.844	2.634
	Br	2.606	2.595	2.639	2.871	2.691	2.922	2.721
	I	2.748	2.689	2.686	3.051	2.720	3.000	2.816

[a] The data refer to 0.111, 0.125, and 0.125 ML coverage for the (111), (110), and (100) surfaces, respectively, corresponding to the structures defined in Figure 1. Distances are in Å.

TABLE 9: Effective Halogen Radius (r_{eff}) for Halogen Chemisorption on the Three Low-Index Surfaces of Cu, Rh, Pd, Ag, Pt, and Au and Average Value ($\langle r_{eff} \rangle$) among the Different Metal Surfaces Derived from Eq 2[a]

		metal						average
	halogen	Cu	Rh	Pd	Ag	Pt	Au	$\langle r_{eff} \rangle$
(111)	F	0.819	0.886	0.867	0.877	0.965	0.946	0.893
	Cl	1.117	1.092	1.049	1.194	1.141	1.223	1.136
	Br	1.263	1.213	1.158	1.316	1.244	1.327	1.253
	I	1.418	1.324	1.265	1.452	1.329	1.426	1.369
(110)	F	1.156	1.228	1.235	1.261	1.306	1.577	1.294
	Cl	1.364	1.343	1.288	1.475	1.440	1.567	1.413
	Br	1.446	1.444	1.315	1.549	1.481	1.622	1.476
	I	1.584	1.464	1.359	1.680	1.389	1.678	1.526
(100)	F	0.940	1.030	1.022	0.988	1.097	1.066	1.024
	Cl	1.211	1.146	1.157	1.304	1.198	1.367	1.231
	Br	1.319	1.235	1.239	1.400	1.282	1.445	1.320
	I	1.461	1.329	1.286	1.580	1.311	1.523	1.415

[a] The data refer to 0.111, 0.125, and 0.125 ML coverage for the (111), (110), and (100) surfaces, respectively, corresponding to the structures defined in Figure 1. Distances are in Å.

TABLE 10: Work Function Change ($\Delta\phi$) Induced by Halogen Chemisorption on the Three Low-Index Surfaces of Cu, Rh, Pd, Ag, Pt, and Au and Average Value ($\langle \Delta\phi \rangle$) among the Different Metal Surfaces[a]

		metal						average
	halogen	Cu	Rh	Pd	Ag	Pt	Au	$\langle \Delta\phi \rangle$
(111)	F	0.456	0.416	0.420	0.582	0.351	0.607	0.472
	Cl	0.238	0.012	0.203	0.514	−0.134	0.377	0.202
	Br	0.156	−0.192	−0.126	0.425	−0.325	0.200	0.023
	I	−0.068	−0.484	−0.397	0.229	−0.649	−0.099	−0.245
(110)	F	0.301	0.224	0.286	0.248	0.045	0.413	0.253
	Cl	0.246	0.091	0.102	0.300	−0.168	0.409	0.163
	Br	0.162	0.057	−0.002	0.232	−0.322	0.284	
	I	0.045	−0.140	−0.146	0.135	−0.668	0.037	−0.123
(100)	F	0.418	0.237	0.444	0.447	0.288	0.526	0.393
	Cl	0.330	−0.090	0.150	0.548	−0.235	0.397	0.183
	Br	0.211	−0.329	−0.051	0.472	−0.451	0.228	0.013
	I	−0.002	−0.626	−0.285	0.366	−0.808	−0.070	−0.238

[a] The data refer to 0.111, 0.125, and 0.125 ML coverage for the (111), (110), and (100) surfaces, respectively, corresponding to the structures defined in Figure 1. Work function changes are in eV.

TABLE 11. Vibrational Frequency ($\nu_\perp$) for the Motion of the Halogen Perpendicular to the Surface for Halogen Chemisorption on the Three Low-Index Surfaces of Cu, Rh, Pd, Ag, Pt, and Au and Average Value ($\langle \nu_\perp \rangle$) among the Different Metal Surfaces[a]

		metal						average
	halogen	Cu	Rh	Pd	Ag	Pt	Au	$\langle \nu_\perp \rangle$
(111)	F	326	317	303	284	293	273	299
	Cl	216	228	217	193	192	189	206
	Br	139	154	150	125	137	124	138
	I	108	127	124	99	117	102	113
(110)	F	202	205	211	196	189	199	200
	Cl	152	129	120	146	123	120	132
	Br	109	94	94	91	89	91	95
	I	82	91	91	76	95	77	85
(100)	F	268	230	275	222	207	260	244
	Cl	176	181	172	151	159	154	166
	Br	122	147	126	116	95	112	120
	I	107	123	116	90	124	88	108

[a] The data refer to 0.111, 0.125, and 0.125 ML coverage for the (111), (110), and (100) surfaces, respectively, corresponding to the structures defined in Figure 1. Frequencies are in cm^{-1}.

However, the anomalous behavior of the I/Au system might also be ascribed to the relativistic effects, which are important for such heavy elements and in part incorporated through the PAW. It is well-known that these effects tend to lead to internuclear distances, which are significantly shorter than those predicted by methods which do not take into account any relativistic effect.[133] Interestingly enough, F adsorption exhibits an opposite trend, with smaller distances found for adsorption on the group 11 metals and larger distances found for adsorption on Pd, Pt, and Rh. Within group 11, the F−metal $r_\perp$ generally increases in the order Cu < Ag < Au. However, in some cases, it is found, similarly to what was observed for the adsorption of I on the group 11 metal surfaces, that $r_\perp$ (Au−F) < $r_\perp$ (Ag−F). Later on, we will use the charges derived from the AIM theory of Bader to rationalize the trends on the metal surface distances. We will show that generally smaller distances are associated with an enhanced covalent character of the interaction and larger distances with a higher degree of ionicity, except for the case of F. By looking at Table 6 with some more detail, one can see, for example, that for the interaction of Cl with the (100) surface $r_\perp$ is 1.74, 1.84, and 1.94 Å, on Cu, Ag, and Au, respectively, and 1.61, 1.65, and 1.70 Å on Rh, Pd, and Pt, respectively. Adsorption of Br on the (100) metal surfaces yields an identical trend with $r_\perp$ of 1.88, 1.98, and 2.04 Å on Cu, Ag, and Au, respectively, and $r_\perp$ of 1.75, 1.76, and 1.83 Å on Rh, Pd, and Pt, respectively. The $r_\perp$ values for I adsorption on the (100) surface follow the order Ag (2.20 Å) > Au (2.16 Å) > Cu (2.07 Å), thus showing again the inversion of the Ag−I, Au−I vertical distances discussed above. A $r_\perp$ value of 1.89 Å is found for Rh, which is very similar to the value (1.88 Å) found for Pt, while a slightly shorter value is found for Pd (1.83 Å). The adsorption of F on the (100) metal surfaces shows an opposite trend, with larger values of $r_\perp$ occurring for the adsorption on the Rh, Pd, and Pt metals (1.42, 1.41, and 1.52 Å, respectively), and smaller values for adsorption of Cu, Ag metals (1.31 and 1.32 Å, respectively). The Au−F $r_\perp$ distance represents an exception with a $r_\perp$ of 1.45 Å, closer to $r_\perp$ on the Rh, Pd, and Pt metals, which is consistent with the explanation given above. Table 6 also shows that, for halogen chemisorption on the (110) surface, $r_\perp$ exhibits almost the same trends discussed above for the (100) surface. Thus, the $r_\perp$ distances for the (110) surface are larger for the group 11 metals

TABLE 12: Adsorption Energy (E_{ads}) for Halogen Chemisorption on the Three Low-Index Surfaces of Cu, Rh, Pd, Ag, Pt, and Au and Average Value ($\langle E_{ads} \rangle$) among the Different Metal Surfaces[a]

		metal						average
	halogen	Cu	Rh	Pd	Ag	Pt	Au	$\langle E_{ads} \rangle$
(111)	F	−4.12	−3.76	−3.42	−3.83	−2.82	−3.00	−3.49
	Cl	−3.35	−3.43	−3.17	−3.09	−2.56	−2.42	−3.00
	Br	−3.05	−3.22	−3.02	−2.83	−2.46	−2.26	−2.81
	I	−2.77	−3.15	−3.03	−2.56	−2.55	−2.14	−2.70
(110)	F	−3.93	−3.51	−3.29	−3.76	−2.66	−2.90	−3.34
	Cl	−3.30	−3.22	−3.14	−3.12	−2.38	−2.38	−2.92
	Br	−3.10	−3.16	−3.16	−2.93	−2.44	−2.27	−2.84
	I	−2.94	−3.38	−3.48	−2.71	−2.89	−2.23	−2.94
(100)	F	−4.22	−3.81	−3.53	−4.01	−2.85	−3.12	−3.59
	Cl	−3.45	−3.73	−3.33	−3.24	−2.70	−2.51	−3.16
	Br	−3.17	−3.61	−3.26	−3.00	−2.73	−2.38	−3.03
	I	−2.92	−3.73	−3.40	−2.73	−3.06	−2.29	−3.02

[a] The data refer to 0.111, 0.125, and 0.125 ML coverage for the (111), (110), and (100) surfaces, respectively, corresponding to the structures defined in Figure 1. E_{ads} values are in eV.

and smaller for the group 10 metals and Rh. This is the case at least for I and Br, for which $r_\perp$ increases monotonically down to the group 11 (1.60 Å < 1.64 Å ≪ 1.77 Å for Cu, Ag, and Au, respectively), whereas for I follows the order 1.88 Å (Ag) ≈ 1.87 Å (Au) > 1.83 Å (Cu). When comparing the rest of metals, Rh, Pt, and Pd, $r_\perp$ for I lies in the sequence 1.57 Å (Pt) > 1.54 Å (Rh) ≫ 1.25 Å (Pd), and for Br, in the sequence 1.58 Å (Rh) ≈ 1.57 Å (Pt) ≫ 1.25 Å (Pd). The $r_\perp$ values for Cl on the M(110) surfaces do not follow the general trend discussed so far in which the $r_\perp$ distances for the group 11 metals are generally larger than for Rh, Pd, and Pt. In fact, for Cl on Pt-(110), $r_\perp$ is 1.49 Å and thus intermediate between that of Cu and Ag that are 1.46 and 1.51 Å, respectively. For Cl, the largest $r_\perp$ value is found for Au (1.66 Å), and the smallest values for Rh and Pd, 1.19 and 1.34 Å, respectively. As for the (100) surface, the smallest $r_\perp$ values for F correspond to Cu and Ag, while larger values are found for Rh, Pd, Pt, and Au, with the largest values occurring as before for adsorption on Pt and Au. Finally, when considering the (111) surface of these metals, the trend displayed by halogens adsorbed on the group 11 metals, exhibiting larger $r_\perp$ distances than when adsorbed on Rh, Pd, and Pt, is found once again for I, and again, $r_\perp$ for I adsorption on Ag is slightly larger than that found for Au. In the case of Br and Cl, it is found that distances for adsorption on Cu are comparable to those obtained for adsorption on Pt and Rh. The complete list of values is reported in Table 6 and will not be further discussed.

To rationalize the trends discussed above for $r_\perp$, it is of interest to compare them with those reported in Table 7 corresponding to the total valence electronic population on the adsorbate measured by numerical integration of the electron density in the space region corresponding to the adsorbate according to the AIM theory of Bader. This comparison will show that, to a certain extent, the trends in distances correlate with the degree of charge transfer from the surface to the adsorbate and hence are governed by the nature of the chemisorption bond. For example, for the (100) surface, it is evident from the values of the charge (calculated as the total Bader population minus the number of halogen valence electrons corresponding to 7) on the adsorbed Br that the interaction of this atomic species with Rh, Pd, and Pt results in rather covalent bonds with an average charge on Br of −0.28 $|e|$, whereas for Cu, Ag, and Au, the interaction has a much larger ionic character with a net charge on Br of −0.47 $|e|$. Thus, for a set of metal surfaces, larger $r_\perp$ distances correspond to the cases where the interaction has a more ionic character. In the case of F, the interaction is always rather ionic, as expected from the large electronegativity of F. Still, there is a small but noticeable variation on going from Cu and Ag, where the Bader net charge is of −0.8 $|e|$, to Rh, Pd, Pt, and Au, where the net charge decreases to −0.7 $|e|$ with a minimum value of −0.64 $|e|$ found for Pt. Note, however, that in this case, the trend found for the charges does not reflect that discussed previously for the distances because the largest $r_\perp$ distance corresponds to the interaction with Pt and here it is associated with the smallest degree of charge separation. Clearly, when the net charges are not largely different, the effect of the atomic size cannot be neglected. This is better illustrated for I adsorption. Here, it is evident that there are three average charge transfers. A transfer of roughly −0.3 $|e|$ describes the interaction of I with Cu and Ag, and a much smaller value of −0.1 $|e|$ is found for the interaction with Au, which nicely correlates with the observation made above that $r_\perp$ (Au−I) < $r_\perp$ (Ag−I) and points out that the interaction of I with Au(100) is essentially covalent in nature. Similarly, it is also found that the interaction of I with Rh(100) and Pd(100) is essentially covalent and even a charge transfer in opposite direction (+0.22 $|e|$) is found for the interaction of I on Pt(100), which is in complete accordance with the very small value computed for $r_\perp$. Here, it is worth pointing out that the positive charge on I is likely to be an artifact arising from the approximate treatment of relativistic effects in these heavy elements. When considering the adsorption of Cl on all M(100) surfaces, the chemisorption bond is characterized by an average transfer of −0.52 $|e|$ except for Pt, where the charge transfer is noticeably smaller (−0.37 $|e|$). In all cases, the interaction of F with these metal surfaces can be defined as essentially ionic, with an average charge transfer of −0.70 $|e|$. Thus, the values of charge transfer for adsorption of F, Cl, Br, and I on Pt(100) compared to the other M(100) surfaces studied in the present work all consistently point toward a more covalent bonding that reaches an inversion of the polarization of the bond in the case of I adsorption. In a similar way, the F, Cl, Br, and I charge values show that Cu and Ag tend to give more ionic bonds, while Au tend to give more covalent bonding, especially with iodine and fluorine. Later on, we will show that this behavior can be fully understood from the metal surface work function values. Let us now continue with the discussion of the charge-transfer distributions obtained for the (111) and (110) surfaces. Table 7 illustrates that the trends are all similar to those discussed above for the (100) surface. The charge-transfer values for the halogen series follows the order Cu, Ag > Rh, Au, Pd > Pt, and adsorption of I on Pt(111) and Pt(110) always results in a charge transfer of about 0.2 $|e|$ in the opposite direction, which once more can be attributed to the approximate treatment of relativistic effects. Again, the interaction of I with Rh, Pd, and Au (111) and (110) surfaces results in an essentially covalent bonding with net charges on I ranging from +0.06 $|e|$ to −0.14 $|e|$. The interactions exhibiting the largest degree of ionicity are found for F adsorption on Cu and Ag with values of roughly −0.7$|e|$. For a given halogen, the most ionic interaction is always that with the Cu and Ag metals and the least ionic is that with the Pt metal. The nature of the halogen−metal interaction for Rh, Au, and Pd is generally intermediate between the two limiting situations represented by Ag, Cu, and Pt. Interestingly enough, this is in agreement with previous cluster model calculations for halogen adsorption on the Ag and Pt surfaces carried out either at the HF level[46,47] or by using a DFT-based method.[53] The cluster model approach seems to be able to

capture the dominant trends, although it will probably fail to describe the behavior along the series, as will be discussed later on. When comparing the charge data for a given halogen on different metals, it is significant to observe that the F adsorption exhibits the smallest variation of the charge transfer (ca. 0.1 $|e|$), whereas I exhibits the largest (ca. 0.5 $|e|$). Thus, generally speaking, the effect of the different metal on the nature of the chemisorption bond is more pronounced for I, intermediate for Br and Cl, and almost inexistent for F. A first consequence is that the interaction of F with metal surfaces could be well described with a simplified jellium model, whereas that of the remaining halogens cannot. To finalize this discussion, let us consider the data listed in the righthandmost column of Tables 6 and 7, which correspond to the average values of $r_\perp$ and charges for each halogen among the different metals. When comparing the different surfaces, it is found that $r_\perp$ follows the (110) > (100) > (111) trend, and the charges for the (110) and (100) surfaces are similar and slightly larger than those computed for the (111) surface. The $r_\perp$ distances increase in the order F < Cl < Br < I as expected. The bonding strength is connected with the degree of bond covalence so that it is found that the degree of ionicity decreases in the order F > Cl > Br > I.

The experimental nearest-neighbor distances can be used to obtain an empirical estimate of the metal−halogen charge transfer, which can be compared to the Bader charges computed in this work. These ionicities are derived on the basis of the halogen effective radius r_{eff} estimated as

$$r_{eff} = r_{NN} - a_0/2\sqrt{2} \qquad (2)$$

where a_0 is the lattice parameter and r_{NN} the halogen−metal nearest-neighbor equilibrium distance, as defined previously. For comparison, the fluorine covalent radius is 0.64 Å and ionic radius is 1.33 Å, the chlorine covalent radius is 0.99 Å and ionic radius is 1.81 Å, the bromine covalent radius is 1.11 Å and ionic radius is 1.95 Å, and the iodine covalent radius is 1.28 Å and ionic radius is 2.16 Å.[74] To facilitate the comparison with the experimental data, Tables 8 and 9 list the r_{NN} and r_{eff} values, respectively, for the system studied. First of all, observe that a correlation between the effective radius in Table 9 and the Bader charges in Table 7 shows up for all metal surfaces except Pt and Au. Again, the different behavior of these two metals can be attributed to relativistic effects.

It has already been mentioned that the most complete set of experimental data concerns Cl and I adsorption on the (111) surface of Cu,[23−27] Rh,[3,28] Pd,[29,30] and Ag.[2,27,31−35] These data refer to a $(\sqrt{3}\times\sqrt{3})$ $R30°$ pattern with 0.33 ML coverage, whereas the theoretical data correspond to 0.11 ML coverage. However, the primary interest here is the variation of bond ionicity for a given adsorbate on different metals, and the overall trend is expected not to be dependent on moderate changes of coverage. This hypothesis will be confirmed by selected calculations carried out for different coverage discussed in the next section. SEXAFS of the $(\sqrt{3}\times\sqrt{3})$ $R30°$ surface for chlorine on Pd(111) and Rh(111) revealed r_{NN} distances of 2.39[29] and 2.38 Å,[28] respectively, although no assignment of the bonding site was made. By using the metal bulk radius and these distances, one obtains an estimate of 1.04 and 1.01 Å for the Cl effective radius on each metal surface. In a similar way, from the r_{NN} values of Cl adsorbed onto Cu(111) and Ag(111), 2.38[127] and 2.70 Å[2], respectively, one obtains effective radii of 1.10 and 1.26 Å, respectively. Now, from a simple interpolation between the covalent (0.99 Å)[74] and ionic radius (1.81 Å)[74] for Cl, one obtains a larger degree of ionicity for the interaction with Ag (32%) and Cu (14%) as compared to Rh (6%) and Pd (3%). This qualitative trend is also found in the Bader charges reported in the present work. This analysis also holds for the interaction of I on various metal surfaces. For instance, in the Pd(111) $(\sqrt{3}\times\sqrt{3})$ $R30°$−I system, a NIXSW study[30] of the structure showed that the I adsorption site is the fcc hollow with an interlayer spacing of 2.16 Å corresponding to a r_{NN} of 2.68 Å, which yields an effective radius of 1.30 Å, thus even smaller than the I covalent radius (1.37 Å).[74] Similar information was obtained from a LEED study[28] of I on Rh(111), which stated that I occupies the fcc 3-fold hollow site with $r_{NN} = 2.71$ Å, leading to an effective radius of 1.37 Å, which coincides with the covalent radius. A similar distance of 2.69 Å was found for the Cu(111)−I r_{NN} distance through SEXAFS experiments,[25] indicating an effective radius for I in the 1.38−1.41 Å range. In these cases, the iodine adsorption leads to a well-ordered $(\sqrt{3}\times\sqrt{3})$ $R30°$ structure at 0.33 ML coverage, although the SEXAFS technique did not permit distinguishing between the two 3-fold sites possible on the (111) surfaces. It is interesting to compare with the case of I adsorption on Ag(111). This system was characterized by a number of techniques,[25,31−35] and all of them consistently found that r_{NN}(Ag−I) is reduced by about 0.1−0.2 Å with respect to Cu, Rh, and Pd. These data suggest an effective radius for I in the range 1.39−1.43 Å, and all are consistent with a much smaller degree of ionic character for the interaction of I with these metal surfaces compared, for instance, with the cases concerning Cl adsorption. Nevertheless, the degree of ionicity is larger for the interaction with Ag (3−8%) and Cu (3−6%) versus Rh (1%) and Pd (<1%). Thus, the present theoretical findings summarized in Table 7 are fully consistent with the trends found on the basis of the empirical estimate of the effective radius. Notice that even the net charge for I on Pd (+0.16 $|e|$) is consistent with the observation that I adsorbed on Pd(111) yields an effective radius that is even smaller than the covalent radius. This can be interpreted as a charge transfer in the opposite direction, thus from the adsorbate to the metal.

The discussion above shows that the structural data contain important information about the degree of covalence or ionicity of halogens adsorbed on the low-index surfaces of various transition metal surfaces. Another property which has been often used to characterize the degree of charge transfer between an adsorbate and a surface is the change of the surface work function induced by the adsorbate.[134,135] The common belief is that adsorbates bearing a positive charge reduce the surface work function, whereas the opposite holds for negatively charged adsorbates. However, Pettersson and Bagus[136] already questioned this interpretation precisely in the study of Cl adsorption on a Cu(100) cluster model. Similar arguments were used later on by Bagus and Illas to justify the large negative charge of O adsorbed on Cu(100) despite the small change in the surface dipole moment induced by the adsorbate, led to a concomitant small change in the work function.[137] That work function changes are not necessarily related to the adsorbate net charge was also shown for the interaction of N on W(100) by Michaelides et al.[138] by using arguments that coincide with those originally given by Pettersson and Bagus. Recently, some of us showed that the interaction of Cl on various metal surfaces lead to negative or positive work function changes, although Cl is always negatively charged.[66] The present work adds further arguments to this interpretation. The data in Table 7 confirm that the net charge of Cl on all the studied metal surfaces is negative and rather large. Results reported in Table 10 confirm once again that the changes in the surface work function induced

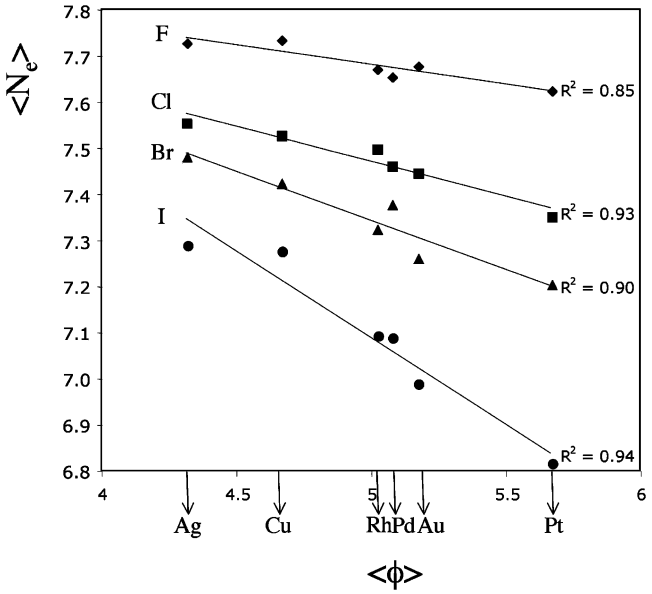

Figure 3. Average halogen total valence Bader population ($\langle N_e \rangle$) on the (111), (110), and (100) metal surfaces as a function of the average metal work function ($\langle \phi \rangle$) for the same three low-index surfaces.

by the presence of an adsorbate cannot always be related to the net charge on this adsorbate. Notwithstanding, one may still argue that, for a given adsorbate, and hence for a given electronegativity or electron affinity, the degree of charge transfer will be dominated by the ability of the metal surface to donate or accept electrons. Hence, for a given adsorbate, one expects a direct relationship between its net charge and the surface work function. Figure 3 reports the average halogen total valence Bader population on the three low-index surfaces as a function of the average metal surface work function for the same low-index surfaces. The almost linear plots indicate that the above argument is indeed correct and permits one to rationalize the charge transfer to the halogens from a quite simple argument. This is one of the key findings of the present systematic study. Notice that the existence of this relationship has implications for the studies of the chemisorption bond based on cluster models because these must provide a relatively accurate prediction of the surface work function. Usually, cluster models for metal surfaces represent adequately the situation in which one electron is removed from the material but hardly represent the opposite situation where one electron is added to the system. In this sense, it is well possible that previous cluster model studies of the interaction of halogens with metal surfaces provide a qualitatively correct description of the chemisorption bond and some local properties. Nevertheless, the present results evidence a clear relationship between the net charge on the adsorbed halogen and the surface work function, which will hardly be predicted by the use of more approximate surface models.

Next, let us turn our attention to the vibrational frequencies corresponding to the normal mode for the vertical displacement of the halogen relative to the surface (Table 11). These are obtained by allowing the adsorbate to move but maintaining the surface atoms fixed at the equilibrium relaxed structure. The trends found for the frequencies essentially reflect those already discussed above for $r_\perp$. For the adsorption of I on the (111) surfaces, the frequency is comparable for Ag and Au (∼100 cm^{-1}), and is slightly higher (108 cm^{-1}) for Cu. The interaction with Pt, Rh, and Pd gives higher frequencies of 117−124 cm^{-1}. For Br, the frequency values follow the order Au, Ag (∼125 cm^{-1}) < Cu, Pt (∼140 cm^{-1}) < Rh, Pd (∼150 cm^{-1}). For Cl, the sequence is Ag, Au, Pt (∼190 cm^{-1}) < Cu, Pd (∼217 cm^{-1}) < Rh (∼228 cm^{-1}). For F, the trend found for $r_\perp$ is not strictly reproduced and the frequency values follow the order Au < Ag < Pt < Pd < Rh < Cu. Thus, globally, the frequency values point out that frustrated translation frequencies are higher for group 10 metals and Rh and lower for group 11 metals, but for Cu and Pt, there is an evident tendency to have higher and lower frequencies, respectively, up to the point that they invert their order (Cl and F cases). The frequencies referring to the (110) surfaces show that also in this case the predicted value for different metals depends essentially on the halogen considered. Thus, the trend found for I is Rh, Pd, Pt (∼90−95 cm^{-1}) > Cu, Ag, Au (∼80 cm^{-1}), thereby following the finding that stronger and more covalent bonds are formed for adsorption onto group 10 metals and Rh. For Br and Cl, the sequence is reversed so that Cu for Br and Cu and Ag for Cl have higher frequencies compared to the other metals. Specifically, for Br, the order is Cu (109 cm^{-1}) > Ag, Au, Rh, Pd, Pt (∼90 cm^{-1}), and for Cl is Cu, Ag (∼150 cm^{-1}) > Rh, Pd, Pt, Au (120−130 cm^{-1}). For F, the frequencies lie in the sequence Rh, Pd (∼210 cm^{-1}) > Cu, Ag, Au (∼200 cm^{-1}) > Pt (190 cm^{-1}). The trends for the (100) surfaces are also similar to those discussed above, and perhaps it is worth commenting that the present calculated values are slightly larger than those previously reported for halogens on Ag(100) using a Hartree−Fock cluster model approach,[45] although the difference can be entirely ascribed to coverage effects.[139]

While there is no extensive information on the vibrational frequencies for the halogens adsorbed on metal surfaces in UHV, the computed trends in vibrational frequencies reproduce those obtained by Mrozek et al.[42] by SERS for analogous systems in an electrochemical environment, except for the case of the heavier metals (i.e., Au, Pt). Because the experiments used polycrystalline surfaces, the comparison is made by considering the metal−adsorbate frequency calculated value averaged over the three surfaces. Similarly to Mrozek et al., we find that, for Br and Cl adsorption, the frequency increases from left to right across the 4d periodic series (i.e., Rh > Pd > Ag). Although the correlation between experiment and theory is rather good with a correlation coefficient of 0.99 for Cl and 0.92 for Br, the deviation from experiment in absolute value is rather large and the vibrational frequencies are underestimated by 37% for Cl and by 32% for Br adsorption. Given the fact that the DFT predicts vibrational frequencies for molecules and adsorbates that are much closer to the experimental ones, the present deviation may be ascribed to the presence of the solvent. Nevertheless, one must keep in mind that the small values of these frequencies correspond to rather flat potential energy curves and hence are also somewhat affected by numerical errors. Also, one needs to consider that Mrozek et al. found that the vibrational frequencies increase from 4d to 5d within a given group (i.e., Au >Ag and Pt > Pd). Data for the Cl−Pd and Pt (111) systems examined in UHV by means of electron energy loss spectroscopy[140,141] showed that this trend is also valid in vacuum. In this case, the present periodic DFT calculations fail in predicting the correct trend, although the vibrational frequency of a given halogen on Ag and Au or on Pd and Pt differ by a few wavenumbers only. This failure should be attributed to the relativistic effects, which are only partially accounted for in the PAW potentials.

The observation that the computed and measured UHV vibrational frequencies exhibit the same trends as those observed in electrochemical environment strongly suggests that the metal surface−halogen bonding in UHV conditions share many

similarities with the electrode−surface halogen bonding. Note that Morzek et al.'s experiments[42] also showed that the vibrational frequencies are significantly blue-shifted with increasing electrode potential, especially for bromide and chloride on Ag and Au, which is symptomatic of partial ionic bonding, whereas this potential dependence is less dramatic for Pt, Pd, and Rh electrodes as expected for a more covalent interaction. Thus the SERS measurements essentially confirm the same periodic trends in the bonding nature as those emerging from our calculations: enhanced bond ionicity for the group 11 metals compared to group 10 and Rh metals, once more pointing out to a possible relation between halogen−metal bonding at the electrochemical interface and in vacuum.

Of particular interest is the discussion of the adsorption energy dependence on the metal and on the particular crystal face. To this end, Table 12 lists the values of E_{ads} for each system studied here. For Cl, Br, and I, it is found that E_{ads} decreases down the group 11 and group 10 metals and also decreases as one progresses from left to right across the 4d and 5d series. For F, a monotonic trend is seen in the group 11 and group 10 metals, whereas the trend found across the 4d series is Ag > Rh > Pd and across the 5d series is Au > Pt. When comparing E_{ads} for the group 11 metals versus the group 10 metals, the E_{ads} values depend on the adsorbate and on the surface plane. The adsorption of I on the (100) surfaces gives the trend Rh > Pd > Pt > Cu > Ag > Au, thus pointing out a stronger surface bond with the Pd, Rh, and Pt metals and a weaker bond with the Cu, Ag, and Au metals. Adsorption of I on the (111) and (110) surfaces gives Rh, Pd > Cu > Pt ≥ Ag > Au, thus mimicking approximately the (100) surface behavior except for the fact that the Cu and Pt values are inverted. For the adsorption of Br on the (110) surfaces, the value for Cu is still lower than that for Rh and Pd, but the value for Pt is intermediate between that for Ag and Au (i.e., Rh, Pd > Cu > Ag > Pt > Au). In other cases, such as Cl and Br adsorption on the (100) metal surfaces and also for Br adsorption on the (111) surfaces, the E_{ads} values on Cu are intermediate between those for Rh and Pd and those for Pt are intermediate between those of Ag and Au (i.e., Rh > Cu ≥ Pd > Ag > Pt > Au). Then one finds two limiting situations, one for the Cl−M(111) systems, where the lowest E_{ads} value corresponds to Pt (i.e., Rh > Cu > Pd > Ag > Au > Pt), and the other one for Cl−M(110), where the highest E_{ads} value corresponds to Cu (i.e., Cu > Rh > Pd, Ag > Pt, Au). Adsorption of F always gives the same sequence corresponding Cu > Ag > Rh > Pd > Au > Pt, showing a reversion of the E_{ads} order for group 10 metals and Rh versus group 11 metals with the exception of Au. Interestingly enough, the trends for halogens on the different metal surfaces confirm a previous conclusion by Koper and Van Santen based on the use of cluster models for the Ag and Pt(111) surfaces.[53] From the analysis of E_{ads}, it is clear that there is no relationship between the interaction energy of a given halogen with a given metal surface and the ionic or covalent nature of the chemisorption bond.

6. Coverage Influence on the Degree of Ionicity

It is also of interest to discuss the metal−halogen bonding dependence on coverage since many studies[5,24,22,142] have reported a change in adsorbate−substrate bond length as function of coverage, which has been interpreted as a change from a more ionic toward a more covalent bonding with increase in coverage. Globally, this change in the bonding mechanism serves to minimize the Coulomb repulsion in the adlayer. For example, one experimental study showed that the Cu(111)−Cl nearest-neighbor distance increases from 2.38 Å at 0.33 ML to 2.48 Å at 0.08 ML,[127] which indicates a change of ionicity from 14 to 26%. The calculations report a distance of 2.39 Å at 0.33 ML coverage and a distance of 2.40 Å at 0.11 ML coverage, thus no substantial bond length change with coverage is observed at least down to 0.11 ML, with a concomitant 3% change only in the bond ionicity (−0.47 $|e|$ versus −0.50 $|e|$). For Ag(111)−Cl, the SEXAFS study by Lamble et al.[2] reported no variation in the nearest-neighbor distance at least down to 0.33 ML coverage. An increase of the Ag−Cl r_{NN} from 2.63 to 2.67 Å with increase in coverage from 0.33 to 0.11 ML is predicted on the basis of the calculations. This small change is essentially associated with a very slight variation in the bond ionicity (from −0.46 $|e|$ to −0.51 $|e|$). A dependence of the surface structure on coverage has also been reported[5] for Cl adsorbed on Cu(100), where the nearest-neighbor Cl−Cu distance was found to be 2.39 for 0.50 ML and 2.42 for 0.12 ML, with Cl effective radius based ionicities of 15 and 19%, respectively. The computed Cu−Cl bond length increases from 2.46 Å at 0.50 ML coverage to −2.50 Å at 0.125 ML coverage and is accompanied with a 1% change in the bond ionicity. Hence, in relative terms, the calculations correctly describe the experimental measured Cl−Cu bond length variation and also provide an estimate of the ionicity variation that approaches that estimated on the basis of the effective radius. Note, however, that in absolute terms, calculations predict larger distances by ∼0.07 Å and higher degrees of ionicity by ∼30−35%. The remaining data relating to the Cl−Cu and Cl−Ag interaction at 0.125 (Table 5) and 0.5 ML coverage (Tables 7, 8) show that the r_{NN} variation is 0.06 Å for Cl−Ag(100), and 0.01 Å for Cl−Ag(110), and no r_{NN} variation for Cl−Cu(100). Comparison of the total populations derived from the Bader analysis shows that variations of r_{NN} are not associated with significant changes in the bond ionicity for the Cu surfaces and to a change of at most 10% for the Ag surfaces. Thus, overall, the data point out that dependence on coverage is larger for Ag compared to Cu in the range of coverage explored in this work. Low coverage was also investigated for the Cu and Pt (100) surfaces. Table 13 summarizes the results obtained for the properties of halogen adsorption on a (3 × 3) supercell, corresponding to 0.056 ML coverage. At low coverage, the bonds are only marginally shorter and the ionicities are very similar to those computed for 0.5 ML coverage. It is seen rather counterintuitively that, for the Pt(100)−halogen series, the larger the metal−halogen bond the lower the ionicity, but again, the differences are really small. A similar effect is seen for I adsorption onto Cu(100). We can conclude that the main trends found in the present study are likely to be valid for a broad range in coverage.

TABLE 13: Adsorption of Cl on Cu(100) and Pt(100) at 0.056 ML[a]

	Cu			Pt		
	r_{NN}	E_{ads}	N_e	r_{NN}	E_{ads}	N_e
F	2.230	−4.29	7.75	2.526	−2.87	7.64
Cl	2.502	−3.55	7.52	2.636	−2.67	7.36
Br	2.619	−3.26	7.41	2.697	−2.69	7.22
I	2.774	−3.00	7.24	2.728	−3.02	6.75

[a] r_{NN} (in Å) is the nearest-neighbor chlorine distance to the surface metal atom. E_{ads} (in eV) is the adsorption energy and N_e is the total valence population (in units of $|e|$) derived from a Bader analysis of the DFT charge density.

7. Conclusions

The present systematic study of the interaction of halogens on the low-index metal surfaces of Cu, Rh, Pd, Ag, Pt, and Au based on density functional theory calculations on periodic slabs reveals some important conclusions, which are summarized as follows:

(i) The present models and methods are able to properly reproduce experimental structural data for the naked surface as well as for ordered phases for which reliable data exists.

(ii) For all metal surfaces, the perpendicular distance of the halogen to the metal surface $r_\perp$ always increases from F to I, the smallest $r_\perp$ values being found for the more open surfaces. However, for a given halogen, the distance to the surface does not follow a monotonic trend. For Cl, Br, and I on metals with incomplete d shells, the $r_\perp$ values are smaller than for the group 11 metal surfaces with a filled d shell. However, for F, the trend is different, with the smallest $r_\perp$ values being found for the interaction with the Cu and Ag surfaces. This in principle unexpected behavior can be understood from the analysis of the chemisorption bond.

(iii) A linear relationship between the surface work function and the total valence electronic population (i.e., the net charge) is found. This explains the dependence of the degree of charge transfer for a given halogen on the metal surface. The larger the surface work function, the smaller the degree of charge transfer. However, one can safely state that the net charge is large for F, intermediate for Cl and Br, and fairly small for I.

(iv) The metal−adsorbate adsorption energies for Cl, Br, and I display the same periodic trend, decreasing down the group 11 and group 10 metals, and decreasing as one progresses from left to right across the 4d and 5d series. For F, the adsorption energies increase within a given group, whereas the trend found across the 4d series is Ag > Rh > Pd and across the 5d series is Au > Pt. When comparing E_{ads} for the group 11 metals versus the group 10 metals, the E_{ads} values depend on the adsorbate and on the surface plane. These trends cannot be explained from simple arguments because they are affected by the nature of the chemisorption bond.

(v) The above conclusions have been found for intermediate coverage, but calculations on representative systems suggest that they are also valid on a rather broad range in coverage.

Finally, let us point out that the present study refers to the adsorption of halogens on metals surfaces in ultrahigh vacuum conditions. However, some qualitative trends can be extracted, such as that the Pt−halogen interaction is more covalent than the group 11 metal−halogen interaction, or trends in metal−halogen vibrational frequencies that are similar to those evident form a SERS study of halide adsorption on transition metal and noble metal electrodes,[42] thereby interrelating to some extent the nature of the metal−halogen bonding in UHV conditions to the metal electrode−halogen bonding.

Acknowledgment. A.M. thanks the European Union for a postdoctoral Marie Curie fellowship (contract MEIF-CT-2003-500155). Financial support has been provided by the Spanish Ministry of Education and Science (projects CTQ2005-08459-CO2-01 and UNBA05-33-001), and in part, by the Generalitat de Catalunya (Projects 2005SGR-00697, 2005 PEIR 0051/69 and Distinció per a la Promoció de la Recerca Universitària de la Generalitat de Catalunya granted to F.I.). Part of the computer time was provided by the Centre de Supercomputació de Catalunya, CESCA, Centre Europeu de Paral.lelisme de Barcelona, CEPBA, and CEBPA-IBM-Research Institute, CIRI, through generous grants from the Universitat de Barcelona, Fundació Catalana per a la Recerca.

References and Notes

(1) Shard, A. G.; Dhanak, V. R. *J. Phys. Chem. B* **2000**, *104*, 2743.
(2) Lamble, G. M.; Brooks, R. S.; Ferrer, S.; King, D. A.; Norman, D. *Phys. Rev. B* **1986**, *34*, 2975.
(3) Shard, A. G.; Dhanak, V. R.; Santoni, A. *Surf. Sci.* **1999**, *429*, 279.
(4) Kadodwala, M. F.; Davis, A. A.; Scragg, G.; Cowie, B. C. C.; Kerkar, M.; Woodruff D. P.; Jones, R. G. *Surf. Sci.* **1995**, *324*, 122.
(5) Kiguchi, M.; Yokoyama, T.; Terada, S.; Sakano, M.; Okamoto, Y.; Ohta, T.; Kitajima, Y.; Kuroda, H. *Phys. Rev B* **1997**, *56*, 1561.
(6) Wang, L.-Q.; Schach von Wittenau, A. E.; Ji, Z. G.; Wang, L. S.; Huang, Z. Q.; Shirley, D. A. *Phys. Rev B* **1991**, *44*, 1292.
(7) Woodruff, D. P.; Seymour, D. L.; McConville, C. F.; Riley, C. E.; Crapper, M. D.; Price, N. P.; Jones, R. G. *Phys. Rev. Lett.* **1987**, *58*, 1460.
(8) Foresti, M. L.; Innocenti, M.; Forni F.; Guidelli, R. *Langmuir* **1998**, *14*, 7008.
(9) Väärtnôou, M.; Pärsimägi, P.; Lust, E. *J. Electroanal. Chem.* **1995**, *385*, 115.
(10) Nazmutdinov, R. R.; Zinkicheva, T. T.; Probst, M.; Lust, K.; Lust, E. *Surf. Sci.* **2005**, *577*, 112.
(11) Goddard, P. J.; Lambert, R. M. *Surf. Sci.* **1977**, *67*, 180.
(12) Westphal, D.; Goldmann, A.; Jona, F.; Marcus, P. M. *Solid State Commun.* **1982**, *44*, 685.
(13) Jona, F.; Westphal, D.; Goldmann, A.; Marcus, P. M. *J. Phys. C: Solid State Phys.* **1983**, *16*, 3001.
(14) Citrin, P. H.; Hamann, D. R.; Mattheiss, L. F.; Rowe, J. E. *Phys. Rev. Lett.* **1982**, *49*, 1712.
(15) Jona, F.; Marcus, P. M. *Phys. Rev. Lett.* **1983**, *50*, 1823.
(16) Chang, C. C.; Winograd, N. *Surf. Sci.* **1990**, *230*, 27.
(17) Zanassi, E.; Jona, F.; Jepsen, D. W.; Marcus, P. M. *Phys. Rev. B* **1976**, *14*, 432.
(18) Zanassi, E.; Jona, F. *Surf. Sci.* **1977**, *62*, 61.
(19) Lamble, G. M.; Brooks, R. S.; Campuzano, J.-C.; King, D. A. *Phys. Rev. B* **1987**, *36*, 1796.
(20) Holmes, D. J.; Panagiotides, N.; Dus, R.; Norman, D.; Lamble, G. M.; Barnes, C. J.; Della Valle, F.; King, D. A. *J. Vac. Sci. Technol., A* **1987**, *5*, 703.
(21) Lamble, G. M.; Brooks, R. S.; King, D. A.; Norman, D. *Phys. Rev. Lett.* **1989**, *6*, 2569.
(22) Winograd, N.; Chang, C.-C. *Phys. Rev. Lett.* **1989**, *62*, 2568.
(23) Crapper, M. D.; Riley, C. E.; Sweeney, P. J. J.; McConvilee, C. F.; Woodruff, D. P. *Surf. Sci.* **1987**, *182*, 213.
(24) Way, W. K.; Pike, A. C.; Rosencrance S. W.; Braun R. M.; Winograd, N. *Surf. Interface Anal.* **1998**, *24*, 137.
(25) Citrin, P. H.; Eisenberger, P.; Hewitt, R. C. *Phys. Rev. Lett.* **1980**, *45*, 1948.
(26) Citrin, P. H.; Eisenberger, P.; Hewitt, R. C. *Phys. Rev. Lett.* **1980**, *47*, 1567.
(27) Citrin, P. H.; Eisenberger, P.; Hewitt, R. C. *Surf. Sci.* **1979**, *89*, 28.
(28) Barnes, C. J.; Wander, A.; King, D. A. *Surf. Sci.* **1993**, *281*, 33.
(29) Shard, A. G.; Dhanak, V. R.; Santoni, A. *Surf. Sci.* **2000**, *445*, 309.
(30) Dhanak, V. R.; Shard, A. G.; D'Addato, S.; Santoni, A. *Chem. Phys. Lett.* **1999**, *306*, 341.
(31) Citrin, P. H.; Eisenberger, P.; Hewitt, R. C. *Phys. Rev. Lett.* **1978**, *41*, 309.
(32) Citrin, P. H.; Eisenberger, P.; Hewitt, R. C. *Phys. Rev. Lett.* **1978**, *41*, 598.
(33) Forstmann, F.; Berndt, W.; Buttner, P. *Phys. Rev. Lett.* **1973**, *30*, 17.
(34) Maglietta, M.; Zanassi, E.; Bardi, U.; Sondericker, D.; Jona, F.; Marcus, P. M. *Surf. Sci.* **1982**, *123*, 141.
(35) Forstmann, F. *Jpn. J. Appl. Phys.* **1974**, *Suppl. 2*, 657.
(36) Iwasita, T.; Nart, F. C. In *Advances in Electrochemical Science and Engineering*; Gerischer, H., Tobias, C. W., Eds.; VCH: Weinheim, 1995; Vol. 4, Chapter 3.
(37) Iwasita, T.; Nart, F. C. *Prog. Surf. Sci.* **1997**, *55*, 271.
(38) Korzeniewski, C. *Crit. Rev. Anal. Chem.* **1997**, *27*, 81.
(39) Rodes, A.; Pérez, J. M.; Aldaz, A. In *Handbook of Fuel Cells: Fundamentals, Technology, and Applications*; Vielstich, W., Lamm, A., Gasteiger, H. A., Eds.; John Wiley: Chichester, U.K., 2003; p 191.
(40) Clavilier, J. *J. Electroanal. Chem.* **1980**, *107*, 211.
(41) Clavilier, J.; Armand, D.; Sun, S. G.; Petit, M. *J. Electroanal. Chem.* **1986**, *205*, 267.
(42) Mrozek, M. F.; Weaver, M. J. *J. Am. Chem. Soc.* **2000**, *122*, 150.
(43) Gao, P.; Weaver, M. J. *J. Phys. Chem.* **1986**, *90*, 4057.
(44) Illas, F.; Sanz, F.; Virgili, J. *J. Electroanal. Chem.* **1982**, *142*, 31.
(45) Illas, F.; Rubio, J.; Ricart, J. M.; Garrido, J. A. *J. Electroanal Chem.* **1986**, *200*, 47.

(46) Bagus, P. S.; Pacchioni, G.; Philpott, M. R. *J. Chem. Phys.* **1989**, *90*, 4287.
(47) Pacchioni, G. *Electrochim. Acta* **1996**, *41*, 2285.
(48) Blanco, M.; Rubio, J.; Illas, F. *J. Electroanal. Chem.* **1989**, *261*, 39.
(49) Rubio, J.; Ricart, J. M.; Casanovas, J.; Blanco, M.; Illas, F. *J. Electroanal. Chem.* **1993**, *359*, 105.
(50) Kramar, T.; Vogtenhuber, D.; Podloucky, P.; Neckel, A. *Electrochim. Acta* **1995**, *40*, 43.
(51) Kuznetsov, An. M. *Electrochim. Acta* **1995**, *40*, 2483.
(52) Ignazak, A.; Gomes, J. A. N. F. *J. Electroanal. Chem.* **1997**, *420*, 71.
(53) Koper, M. T. M.; van Santen, R. A. *Surf. Sci.* **1999**, *422*, 118.
(54) Bagus, P. S.; Hermann, K.; Bauschlicher, C. W., Jr. *J. Chem. Phys.* **1984**, *81*, 1966.
(55) Bagus, P. S.; Hermann, K. *Phys. Rev. B* **1986**, *33*, 2987.
(56) Bagus, P. S.; Illas, F. *J. Chem. Phys.* **1992**, *96*, 8962.
(57) Nelin, C. J.; Bagus, P. S.; Philpott M. R. *J. Chem. Phys.* **1987**, *87*, 2170.
(58) Illas, F.; Rubio, J.; Ricart, J. M. *J. Mol. Struct. (THEOCHEM)* **1993**, *287*, 167.
(59) Marquez, A. M.; López, N.; García-Hernández, M.; Illas, F. *Surf. Sci.* **1999**, *442*, 463.
(60) Bagus, P. S.; Illas, F. In *Encyclopedia of Computational Chemistry*; Schleyer, P. v. R., Allinger, N. L., Clark, T., Gasteiger, J., Kollman, P. A., Schaefer, H. F., III, Schreiner, P. R., Eds.; John Wiley & Sons: Chichester, UK, 1998; Vol. 4, p 2870.
(61) Whitten, J. L.; Yang, H. *Surf. Sci. Rep.* **1996**, *24*, 59.
(62) Pacchioni, G. *Heterog. Chem. Rev.* **1996**, *2*, 213.
(63) Doll, K.; Harrison, N. M. *Phys. Rev. B* **2001**, *63*, 165410.
(64) de Leeuw, N. H.; Nelson, C. J.; Catlow, C. R. A.; Sautet, P.; Dong, W. *Phys. Rev. B* **2004**, *69*, 045419.
(65) Doll, K.; Harrison, N. M. *Chem. Phys. Lett.* **2000**, *317*, 282.
(66) Migani, A.; Sousa, C.; Illas, F. *Surf. Sci.* **2005**, *574*, 297.
(67) Wang, Y.; Wang, W.; Fan, K.; Deng, J. *Surf. Sci.* **2001**, *487*, 77.
(68) Kresse, G.; Hafner, J. *Phys. Rev. B* **1993**, *47*, 558.
(69) Kresse, G.; Hafner, J. *Phys. Rev. B* **1993**, *47*, 13115.
(70) Kresse, G.; Hafner, J., *Phys. Rev. B* **1994**, *47*, 14251.
(71) Perdew, J. P.; Wang, Y. *Phys. Rev. B* **1992**, *45*, 13244.
(72) Perdew, J. P.; Burke, K.; Ernzerhof, M. *Phys. Rev. Lett.* **1996**, *77*, 3865.
(73) Ceperley, D. M.; Alder, B. J. *Phys. Rev. Lett.* **1980**, *45*, 566.
(74) Kittel, C. *Introduction to Solid State Physics*, 6th ed.; Wiley: New York, 1986.
(75) Wyckoff, R. W. G. *Crystal Structures*, 2nd ed.; Interscience Publishers: New York, 1965; Vol. 1.
(76) Blöchl, P. E. *Phys. Rev. B* **1994**, *50*, 17953.
(77) Kresse, G.; Joubert, D. *Phys. Rev. B* **1998**, *59*, 1758.
(78) Bader, R. F. W. *Atoms in Molecules: A Quantum Theory*; Oxford University Press: New York, 1990.
(79) Fowler, D. E.; Barth, J. V. *Phys. Rev. B* **1995**, *52*, 2117.
(80) Jiang, Q. T.; Fenter, P.; Gustafsson, T. *Phys. Rev. B* **1991**, *44*, 5773.
(81) Davis, H. L.; Noonan, J. R. *J. Vac. Sci. Technol.* **1982**, *20*, 842.
(82) Noonan, J. R.; Davis, H. L. *J. Vac. Sci. Technol.* **1980**, *17*, 194.
(83) Davis, H. L.; Noonan, J. R. *Surf. Sci.* **1983**, *126*, 245.
(84) Adams, D. L.; Landman, U. *Phys. Rev. B* **1977**, *15*, 3775.
(85) Lind, D. M.; Dunning, F. B.; Walters, G. K. *Phys. Rew. B* **1987**, *35*, 9037.
(86) Quinn, J.; Li, Y. S.; Tian, D.; Li, H.; Jona, F.; Marcus, P. M. *Phys. Rev. B* **1990**, *42*, 11348.
(87) Quinn, J.; Li, Y. S.; Tian, D.; Li, H.; Jona, F.; Marcus, P. M. *Phys. Rev. B* **1991**, *43*, 7305.
(88) Oed, W.; Dötsch, B.; Hammer, L.; Heinz, K.; Müller, K. *Surf. Sci.* **1998**, *207*, 55.
(89) Adams, D. L.; Nielsen, H. B.; Andersen, J. N.; Stensgaard, I.; Feidenhans'l, R.; Sørensen, J. E. *Phys. Rev. Lett.* **1982**, *49*, 669.
(90) Noonan, J. R.; Davis, H. L.; Jenkins, L. H. *J. Vac. Sci. Technol.* **1978**, *15*, 619.
(91) Davis, H. L.; Noonan, J. R.; Jenkins, H. *Surf. Sci.* **1979**, *83*, 559.
(92) Noonan, J. R.; Davis, H. L. *Surf. Sci.* **1980**, *99*, L424.
(93) Kuk, Y.; Feldman, L. C. *Phys. Rev. B* **1984**, *30*, 5811.
(94) Chang, C.-C.; Winograd, N. *Phys. Rev. B* **1989**, *39*, 3467.
(95) Holub-Krappe, E.; Horn, K.; Frenken, J. W. M.; Kraus, R. L.; Van der Veen, J. F. *Surf. Sci.* **1987**, *188*, 335.
(96) Chan, C.-M.; Cunningham, S. L.; van Hove, M. A.; Weinberg, W. H. *Surf. Sci.* **1977**, *67*, 1.
(97) Alff, M.; Moritz, W. *Surf. Sci.* **1979**, *80*, 24.
(98) Noonan, J. R.; Davis, H. L. *Vacuum* **1982**, *32*, 107.
(99) Maglietta, M.; Zanassi, E.; Jona, F.; Jepsen, D. W.; Marcus, P. M. *J. Phys. C* **1977**, *10*, 3287.
(100) Chae, K. H.; Lu, H. C.; Gustafsoon, T. *Phys. Rev. B* **1996**, *54*, 14082.
(101) Lindgren, S. Å.; Walldén, L.; Rundgren, J.; Westin, P. *Phys. Rev. B* **1984**, *29*, 576.
(102) Watson, P. R.; Shepherd, F. R.; Frost, D. C.; Mitchell, K. A. R. *Surf. Sci.* **1978**, *72*, 562.
(103) Tear, S. T.; Röll, K.; Prutton, M. *J. Phys. C: Solid State Phys.* **1981**, *14*, 3297.
(104) Woodruff, D. P.; Mitchell, K. A. R.; McDonnel, L. *Surf. Sci.* **1974**, *42*, 355.
(105) Reid, R. J. *Surf. Sci.* **1972**, *29*, 603.
(106) Statiris, P.; Lu, H. C.; Gustafsson, T. *Phys. Rev. Lett.* **1994**, *72*, 3574.
(107) Soares, E. A.; Leatherman, G. S.; Diehl, R. D.; Van Hove, M. A. *Surf. Sci.* **2000**, *468*, 129.
(108) Botez, C. E.; Elliott, W. C.; Miceli, P. F. *Phys. Rev. B* **2001**, *63*, 113404.
(109) Barbieri, A.; Van Hove, M. A.; Somorjai, G. A. *Surf. Sci.* **1994**, *306*, 261.
(110) Hengrasmee, S.; Mitchell, K. A. R.; Watson, P. R.; White, S. J. *Can. J. Phys.* **1980**, *58*, 200.
(111) Feder, R.; Pleyer, H.; Bauer, P.; Müller, N. *Surf. Sci.* **1981**, *109*, 419.
(112) Van der Veen, J. F.; Smeenk, R. G.; Tromp, R. M.; Saris, F. W. *Surf. Sci.* **1979**, *79*, 219.
(113) Davies, J. A.; Jackson, D. P.; Norton, P. R.; Posner, D. E.; Unertl, W. N. *Solid State Commun.* **1980**, *34*, 41.
(114) Bøgh, E.; Stensgaard, I. *Phys. Lett. A* **1978**, *65*, 357.
(115) Adams, D. L.; Nielsen, H. B.; Van Hove, M. A. *Phys. Rev. B* **1979**, *20*, 4789.
(116) Kesmodel, L. L.; Stair, P. C.; Somorjai, G. A. *Surf. Sci.* **1977**, *64*, 342.
(117) Stair, P. C.; Kaminska, T. J.; Kesmodel, L. L.; Somorjai, G. A. *Phys. Rev. B* **1975**, *11*, 623.
(118) Kesmodel, L. L.; Somorjai, G. A. *Phys. Rev. B* **1975**, *11*, 630.
(119) Felter, T. E.; Sowa, E. C.; Van Hove, M. A. *Phys. Rev. B* **1989**, *40*, 891.
(120) Ohtani, H.; Hove, M. A.; Somorjai, G. A. *Surf. Sci.* **1987**, *187*, 372.
(121) Tyson, W. R.; Miller, W. A. *Surf. Sci.* **1977**, *62*, 267.
(122) Michaelson, H. B. *J. Appl. Phys.* **1977**, *48*, 4729.
(123) Rovida, G.; Pratesi, F. *Surf. Sci.* **1975**, *51*, 270.
(124) Schott, J. H.; White, H. S. *J. Phys. Chem.* **1994**, *98*, 291.
(125) Andryushechkin, B. V.; Eltsov, K. N.; Shevlyuga, V. M.; Yurov, V. Yu. *Surf. Sci.* **1988**, *407*, L633.
(126) Bowker, M.; Waugh, K. C. *Surf. Sci.* **1983**, *134*, 639.
(127) Way, W. K.; Pike, A. C.; Rosencrance, S. W.; Braun, R. M.; Winograd, N. *Surf. Interface Anal.* **1998**, *24*, 137.
(128) Woodruff, D. P.; Seymour, D. L.; McConville, C. F.; Riley, C. E.; Crapper, M. D.; Prince, N. P. *Surf. Sci.* **1988**, *195*, 237.
(129) Crapper, M. D.; Riley, C. E.; Sweeney, P. J. J.; McConville, C. F.; Woodruff, D. P. *Europhys. Lett.* **1986**, *2*, 857.
(130) Dirac, P. A. M. *Proc. Cambridge Philos. Soc.* **1930**, *26*, 376.
(131) Slater, J. C. *Phys. Rev.* **1951**, *81*, 385.
(132) Hammer, B.; Hansen, L. B.; Norskov, J. K. *Phys. Rev. B* **1999**, *59*, 7413.
(133) Pyykko, P. *Chem. Rev.* **1988**, *88*, 563.
(134) Lang, N. D. *Surf. Sci.* **1983**, *127*, L118.
(135) Zangwill, A. *Physics at Surfaces*; Cambridge University: Cambridge, 1988.
(136) Pettersson, L. G. M.; Bagus, P. S. *Phys. Rev. Lett.* **1986**, *56*, 500.
(137) Bagus, P. S.; Illas, F. *Phys. Rev. B* **1991**, *42*, 10852.
(138) Michaelides, A.; Hu, P.; Lee, M.-H.; Alavi, A.; King, D. A. *Phys. Rev. Lett.* **2003**, *90*, 246103.
(139) Vilaseca E.; Illas, F. *Chem. Phys. Lett.* **1989**, *159*, 165.
(140) Zhou, X.-L.; Liu, Z.-M.; Kiss, J.; Sloan, D. W.; White, J. M. *J. Am. Chem. Soc.* **1995**, *117*, 3565.
(141) Aarts, J. F. M.; Phelen, K. G. *Surf. Sci.* **1989**, *222*, L853.
(142) Lamble, G. M.; Brooks, R. S.; King, D. A.; Norman, D. *Phys. Rev. Lett.* **1988**, *61*, 1112.